Adhesion Contact Deformation in Nanobridge Tests

*Yao Gao[1,2], San-Qiang Shi[2] and Tong-Yi Zhang[1,]**

1 Shanghai Materials Genome Institute and Shanghai University Materials Genome Institute, Shanghai University, 99 Shangda Road, Shanghai, China

[2] Department of Mechanical Engineering, The Hong Kong Polytechnic University, Hung Hom, Kowloon, Hong Kong, China

Keywords: Adhesion contact deformation, Nanobridge tests, Atomic force microscopy, Young's modulus, Size effect

* To whom correspondence should be addressed: mezhangt@ust.hk and zhangty@shu.edu.cn

An accurate grasp of the mechanical properties, especially Young's moduli, of one dimensional nanomaterials plays a crucial role in the design and safe service of flexible electronic devices and implanted biomedical sensors. Nanobridge tests are widely used in the characterization of the mechanical properties of nanowires. In these tests, an atomic force microscope (AFM), functioning as a test machine, exerts a force to bend a nanowire suspended across a trench or a hole with the two ends fixed on a template or substrate. Adhesion contact deformation occurs inevitably during nanobridge testing between the AFM tip and the tested sample, thereby underestimating the

Young's modulus of the tested nanowire and causing a pseudo-size effect in the determined Young's modulus. The present work systematically investigates the adhesion contact deformation in nanobridge tests and provides an analytical approach to evaluate the contact deformation and to determine the Young's modulus. To illustrate the developed methodology, AFM nanobridge tests were conducted on gold nanowires (180–340 nm wide, 3.6–5.1 μm long and 90 nm thick). The results indicate that when the contact deformation was taken into consideration, the average Young's modulus increased by 4.63%. Guidelines for minimizing the impact of contact deformation in practical experiments are presented. Furthermore, the results provide insight into the probable causes of the variation in experimentally obtained size-dependencies of Young's moduli of nanowires.

Introduction

One-dimensional (1D) nanomaterials, such as nanowires, nanofibers, and nanotubes, have much longer lengths than their diameters or cross section dimensions. Usually, when the diameter or cross section size of a 1D material is smaller than 100 nm, the 1D material is called the 1D nanomaterial. It is also very often to call these 1D materials as 1D nanomaterials when their diameters or cross section sizes are smaller than 500 nm. In the present work, the investigated Au beams have cross section sizes smaller than 500 nm and are called Au nanowires for convenience. One-dimensional (1D) nanomaterials have been widely used as building blocks in nano/microelectromechanical systems (N/MEMSs),[1, 2] nano/microgenerators,[3, 4] wearable sensors,[5] flexible nano/microelectronic devices, etc. due to their fascinating properties.[6-8] Young's modulus is one of the most important mechanical properties of solid materials, which gives the relationship between stress and strain in the linear elastic region. Accurate values of Young's moduli of materials are prerequisites in the design, manufacture, and performance of various

devices, structures, and machines made from these materials. In particular, N/MEMSs, such as biomedical N/MEMSs and biomedical implants, etc, use 1D nanomaterials as their building blocks and thus requests, in advance, accurate values of Young's moduli. Inaccurate Young's modulus values of 1D nanomaterials can lead to unexpected errors and failures of biomedical N/MEMSs and biomedical implants that may be disastrous to patients.

Mechanically characterizing Young's modulus of 1D nanomaterials becomes increasingly difficult as their diameters or cross-section sizes decrease. Earlier research results[9-12] show that the Young's modulus of 1D nanomaterials depends strongly on their diameters or cross-section sizes, and that this "size effect" plays a key role in designing N/MEMSs with predictable and reproducible performance. Various experimental techniques have been developed to measure Young's modulus of 1D nanomaterials, including in-situ microscopy uniaxial tensile tests, dynamic resonance tests, nanoindentation tests, microbridge tests and nanobridge (NB) tests, etc. Atomic force microscopes (AFMs) can function as mechanical testingmachines, with which Young's modulus of a material can be measured by using the contact loading mode and the tapping mode. The Young's modulus measured with the tapping mode is very much localized and therefore the tapping mode is often used to map Young's modulus over an interested area of a tested sample. The tapping results, however, depend strongly on the local testing conditions such as the AFM tip radius and the surface roughness of a tested sample. Alternately, the contact loading mode may conduct uniaxial tensile test and bending test on samples having micrometers in length and the measured Young's modulus is the averaged value over the entire tested sample. The AFM conducted uniaxial tensile tests and bending tests mimic the conventional uniaxial tensile tests and bending tests, respectively, and therefore, the testing results are more reliable in engineering sense. For example, the elastic and

adhesive properties of alkanethiol self-assembled monolayers on gold were investigated[13] by using the AFM contact loading mode and the unloading load-displacement was analyzed with the solution developed by Xu and Pharr[14]. Their results show that the elastic modulus of the monolayer film decreases from 1.0 to 0.15 GPa and the work of adhesion increases from 82.8 to 168.3 mJ m^{-2}, as the chain length of the alkanethiol decreases from 18 to 5.13 The AFM contact mode is also adopted in the present work to carry out nanobridge (NB) tests, where a tested nanobeam is suspended over a trench or a hole with its two ends clamped on a substrate or a template. NB tests have been extensively performed to evaluate the Young's moduli of nanowires (NWs),[9, 15-22] and the test reliability and accuracy have been improved by reliably clamping the NWs' two ends and by bending at multiple locations instead of just at the center.[20, 23] However, many values of the Young's moduli of NWs extracted from the NB tests are smaller than the corresponding values of their bulk counterparts with the same crystal structure, and smaller than the values measured from other techniques.[20, 24] For instance, the evaluated averaged values of Young's moduli from nanobridge tests for Au (diameter/width: 40-340 nm) and Ag (diameter: 45.6-60.4 nm) nanowires range from 70 to 75 GPa[20, 24] and 15.4 to 24.6 GPa[23], respectively; smaller than their bulk values (Au: 79 GPa, Ag: 83 GPa)[25] and the values obtained from nanoindentation tests for Ag nanowires (88 ± 5 GPa)[26]. The huge underestimation of the Young's modulus of Ag nanowires[21] measured from the bending tests might be caused by the three reasons: 1) inaccurately positioning the AFM tip right at the NB's center, 2) loose clamp of NB's two ends to the substrate (or template), which could lead to slippage at the two ends during the bending test, and 3) the neglect of substrate deformation and residual stress in the analysis. In contrast, these three unreliable reasons have been addressed in the measurement of Young's modulus on Au nanowires[22] and thus the measured value of Young's modulus is more reliable, where the small underestimation of the Young's

modulus might be caused by the adhesion contact deformation between the probe tip and the tested sample, which is studied in the present work. In addition, there is great inconsistency in the experimentally observed size-dependent Young's moduli of NWs. For example, Young's moduli of ZnO NWs were found to either increase[11, 12] or remain unchanged[11, 12, 18] with decreased diameters, and Young's moduli of Si NWs were found to either increase[9, 19], decrease[27] or be unaffected[16] when diameters decreased. The size-dependent Young's modulus may be induced by crystalline defects, such as grain boundaries[28], crystalline surfaces, which depend on the surface orientation[29], the facets, edges, shape, and symmetry of nanomaterials[30-32].

A deep understanding of the mechanism of the size-dependent Young's modulus relies on the reliable experimental results. Although there are various experimental methods to determine the Young's modulus, the present work focuses on the NB test. As mentioned above, slippage at clamped ends, substrate deformation, and/or adhesion contact deformation during NB tests may lead to underestimation and unreliable assessment of size-dependent Young's moduli. The slippage can be avoided by reliably preparing the tested samples.[20] The substrate deformation has been systematically investigated.[20, 21, 33] However, the influence of adhesion contact deformation on bending tests has not been comprehensively studied aside from one theoretical analysis.[21] The present study combines experimental investigation and theoretical consideration to comprehensively explore the adhesion contact deformation in NB tests, with the aim to further improve the NB tests and to clarify the inconsistency in experimentally measured size dependency of Young's moduli in NWs. The adhesion contact deformation depends greatly on the AFM tip radius and the surface roughness of a tested sample, as described in the classic book, Contact Mechanics[34]. To elucidate the adhesion contact deformation, pure contact tests were also carried

out in the present study on supported Au NW samples by using the same AFM tip as that used in the NB tests. The supported Au NW samples were fabricated with the identical NB sample fabrication conditions, except that the substrate of the supported Au NW samples was not etched away, so that the surface roughness of the supported Au NW samples must be more or less the same as that of NB samples.

There are many theoretical models for adhesion contact. For example, the Johnson–Kendall–Roberts (JKR) model[35] and Derjaguin–Muller–Toporov (DMT) model[36] are well known for adhesion contact with elastic deformation. Contacted solids can go through elastic-plastic deformation, and only a few models take the resultant adhesion into account. The elastic-plastic adhesion models include (1) the Thornton and Ning (TN) model[37], which extends the JKR model to the plastic region; (2) the Maugis and Pollock (MP) model[38], which adopts the JKR model in both the elastic region and the unloading process while treating the adhesion force as a constant in the fully plastic region; and (3) the Kogut and Etsion (KE) model[39], which extends the DMT model to the elastic-plastic region and derives a numerical solution for the adhesion force using the finite element method (FEM). The challenge here is that none of these elastic-plastic adhesion contact models is universal. NB tests must be carefully examined experimentally and compared with the theoretical models. In this work, a methodology is developed to examine experimentally measured jump-in and pull-off forces. This should allow the load-deflection curves of NB tests to be analyzed under consideration of adhesion contact deformation.

Experimental

The suspended Au NB samples were fabricated via a hybrid Ebeam lithography and photolithograph method (see details in the ESI). The fabrication of supported Au NW samples followed the same process flow as that used for Au NBs except of the etching step. The typical dimensions of the Au NB and NW samples were 180-340 nm wide, 3.6-5.1 μm long and ~90 nm thick. The scanning electron microscope images of the fabricated suspended Au NB and supported Au NW are shown in Figures 1(a1) and (a2), respectively. Both images suggest uniform width distribution along the length direction. Before each test, the quality of the samples was examined via scanning electron microscopy and atomic force microscopy. Based on these scanning images, the surface roughness RRMS of our tested NB and supported NW samples are evaluated to be 6.65±1.63 nm and 6.36±1.25 nm, respectively. The insets at the upper left corners of Figures 1(a1) and (a2) are AFM scanning images showing where the scanning lines are selected, and the corresponding height profiles are illustrated in the insets at the bottom left corners of Figures 1(a1) and (a2), respectively. For the Au NW sample, the height difference between the plateau region of curves BB' is 92 nm, which is very close to the preset thickness value (90 nm) and indicates the high quality control of the fabrication process. For the NB sample, the height difference between the plateau region of curves AA' is 380 nm. As the thickness of the NB is only ~90 nm, the fabricated Au NB is suspended as a bridge. The deflection sensitivity of the AFM testing system was calibrated on an alumina wafer (E: 369 -463GPa)[40] before and after each test. The employed AFM tips (Bruker MPP-21120-10) had an original tip radius of 8 nm and were made of phosphorous doped silicon with a Young's modulus of 165 GPa and mounted on a rectangular cantilever. The AFM tip wore quickly at the first hundreds of tests and after about 900 tests, the tip radius was changed very slowly and could be regarded as a constant approximately. The experimental data were used only when the tip radius reached an approximate constant value. The

cantilever's spring constant was calculated using the thermal noise method and had a value of 3±0.017 N/m. In the NB bending tests, the bending load was applied to the tested sample vertically by moving the sample stage up and down while keeping the AFM tip stationary, as illustrated in Figure 1(b1). The loading and unloading rates were set to be the same at 20 nm/s. To avoid the axial tensile stretch of the NW, the bending deflections were kept smaller than half the thickness of the NW to achieve the nominal linear elastic bending behaviour.[16, 41] Pure contact tests were conducted on the Au NW samples with the same kind of AFM tip cantilever and at the same loading and unloading rate, as illustrated in Figure 1(b2).

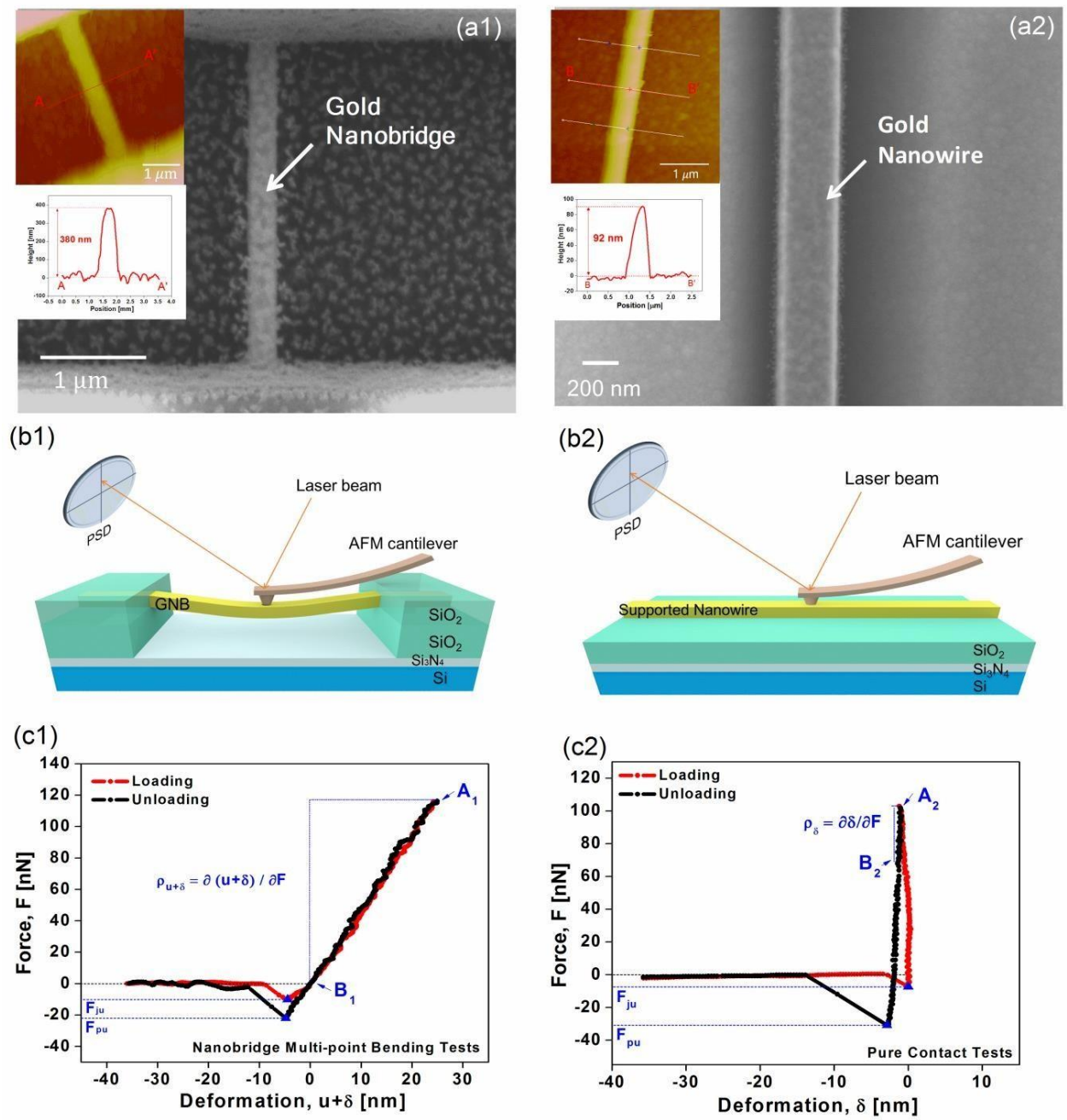

Figure 1 (a) SEM images of a fabricated Au NB (a1) and a fabricated Au NW (a2). The insets at the upper left corner are AFM surface scan images of a fabricated Au NB and a fabricated Au NW, respectively. In both AFM images, section lines are selected across the NB/NW's width direction extending to the substrate marked AA' and BB', respectively. The corresponding height profiles to section lines AA' and BB' are provided in insets at the bottom left corner, respectively. (b) Schematic illustration of the NB bending tests (b1) and the pure contact tests (b2). (c) The entire loading and unloading curves on the Au NB (c1) and on

the Au NW (c2), where A1 and A2 are the points with the preset maximum load and associated displacement, B1 is the point with the zero external load and associated displacement and B2 is the point with two thirds of the preset maximum load and associated displacement.

Results and discussion

Figures 1(c1) and (c2) show a typical load-deflection curve of the NB test and pure contact test, respectively, illustrating the jump-in force F_{ju} and the pull-off force F_{pu} due to adhesion contact in addition to the unloading compliances ρ. The curvature radius R of adhesion contact was calculated based on the jump-in forces using the following equation[42]:

$$R = \frac{8}{9H_A k_c^2}\left|F_{ju}\right|^3 \quad (1)$$

where kc is the spring constant of the AFM cantilever and H_A is the Hamaker constant (~0.38 × 10−18 J).[43] Figure 2(a) shows the jump-in force F_{ju} against the test number for a used AFM tip, which varied its tip curvature from the brand-new shape state to the blunt state, indicating that after 900 tests the jump in force F_{ju} could be approximately treated as a constant of 9.93 nN. The curvature radius R of adhesion contact for the blunting of the AFM tip was calculated as 254.49 nm. The value of pull-off force F_{pu} for a two-body contact system depends on the maximum load F_{max}. Plastic deformation occurred during contact, leading to a change in the contact curvature from R to R', as illustrated in the inset of Figure 2(b). The solid circles in Figure 2(b) plot the experimentally obtained pull-off force versus the applied maximum load. Obviously and surprisingly, the pull-off force F_{pu} increased with the increase of the applied maximum load F_{max} , and even the highest applied maximum load was lower than 200 nN. In the experiment, as shown

in Figure 1(c2), the pure contact compliance ρ_δ was determined by linear fitting the upper third of the unloading curve in the contact test (from point A2 to point B2). The experimentally measured $F_{max} - \rho_\delta$ relationship and $F_{pu} - \rho_\delta$ relationship are plotted as solid circles in Figures 2(c) and (d), respectively. The red solid lines in Figures 2(b)-(d) are the fitting curves based on the TN model[37]. Overall,[14] adhesion elastic-plastic contact models were used to fit the experimental data (see details in the ESI).

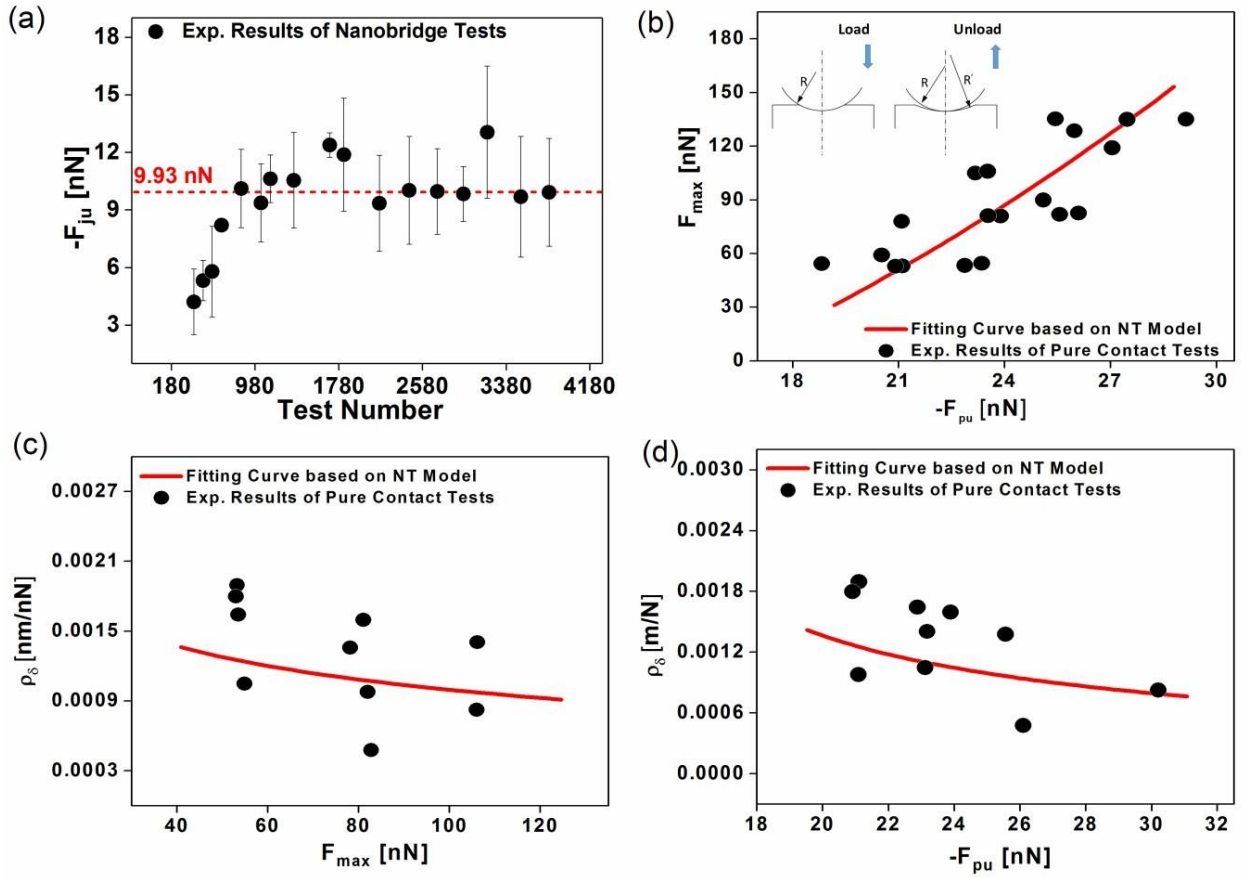

Figure 2 (a) Experimentally obtained jump-in force F_{ju} against test number for one single AFM tip. (b) Experimental results (solid black circles) and fitting curve (red) based on the TN adhesion contact model of pull-off force F_{pu} versus maximum applied load F_{max} from pure bending tests. The inset shows an illustration of the contact curvature change when plastic deformation occurred during the contact. (c) Experimental results (solid black circles) and fitting curve (red) based on the TN adhesion contact model

of contact unloading compliance ρ_δ versus F_{max} from pure contact tests. (d) Experimental results (solid black circles) and fitting curve (red) based on the TN adhesion contact model of ρ_δ versus F_{pu} from pure contact tests.

As the TN model fits the experimental data better than the others, it is adopted in the following analysis. The pull-off forces versus the maximum applied load obtained from the NB bending tests are plotted in Figure S3 in the ESI. The averaged value of F_{pu} from the NB test under a given maximum loading force is consistent with that from the pure contact test and the predicted value from the TN model under the same F_{max}. The least square fitting of experimental data of $F_{pu} - F_{max}$, $F_{max} - \rho_\delta$ and $F_{pu} - \rho_\delta$ with the TN model determines the average Young's modulus of the samples, the work of adhesion Γ and the effective yield strength Y to be 79.28 GPa, 0.013 N/m and 0.26 GPa, respectively. The fitted Young's modulus of Au is 79.28 GPa, which is consistent with the reference value (~79 GPa) for bulk Au[25]. As the AFM tip is made of silicon (yield strength: ~7 GPa[44]) and therefore has a much greater yield strength than the Au NB, the effective yield strength can be approximated as the yield strength of the Au NB. According to the experimental results reported by Espinosa and Prorok[45], the yield strength of the Au thin films is size dependent, ranging from 0.055 to 0.22 GPa and increasing with the reduce of film thickness and width for the width from 20 to 2.5 μm and the thickness from 1.0 to 0.3 μm. Considering the present Au NB samples had much smaller width (180-340 nm) and thickness (90 nm), the evaluated value of 0.26 GPa for yield strength is consistent with the reported experimental results. In multi-point NB bending tests, a vertical bending test is carried out at several positions along the length direction of one NB sample. Young's modulus is extracted from the compliance–testing position relationship.[17] The experimentally measured compliance in NB tests is $\rho_{u+\delta} = \partial(u + \delta)/\partial F$, where u and δ denote the displacements induced by beam bending and adhesion contact, respectively.

The measured bending compliance is the slope of the deflection relative to the bending load and is experimentally determined by a linear fitting of the unloading curve from points A1 to B1, as illustrated in Figure 1(c1).

Let E_u and $E_{u+\delta}$ denote the Young's modulus of the sample obtained by considering and neglecting the influence of adhesion contact deformation, respectively. For each Au NB sample, the value of $E_{u+\delta}$ is obtained by directly fitting the experimentally obtained $\rho_{u+\delta} - a$ relationship to NB test theory[20]. The value of E_u is obtained by fitting the experimentally measured $\rho_{u+\delta} - a$ relationship to the TN–NB test combined model. For each testing location a, the $u - F$and $\delta - F$ relationships are generated according to NB test theory and the TN model, respectively. Then, the $(u + \delta) - F$ relationship of the test site is obtained by superposition, and the unloading compliance $\rho_{u+\delta^*}$ is obtained by linear fitting the $(u + \delta) - F$ curve. The optimum value for Eu can be determined by comparing the fitted $\rho_{u+\delta*}$ to the experimentally measured $\rho_{u+\delta}$. As an illustration, the experimentally obtained $\rho_{u+\delta} - a$ relationships from three different Au NB samples together with the fitting curves for E_u and $E_{u+\delta}$ are presented in Figure 3(a). According to this method, the experimental results reported in the previous work[20] are reanalyzed, and the results are plotted in Figure 3(b). After considering the influence of contact deformation, the averaged Young's modulus value increases by 4.63% from 75.35±7.87 GPa to 78.84±9.42 GPa. This value of 78.84 GPa is very close to that of 79.28 GPa, which is obtained by fitting the pure contact test results to the TN model as shown in Figures 2(b)-(d). Figure 3(b) indicates also that the averaged Young's modulus increases slightly as the width of the sample deceases. When the cantilever's spring constant is 3.017 N/m, the final extracted Young's modulus for Au NWs is 80.10±9.17 GPa, which is 1.59% higher than the value of 78.84±9.42 GPa of spring constant 3 N/m. When the cantilever's

spring constant is 2.983 N/m, the final extracted Young's modulus for Au NWs is 77.57±8.78 GPa, which is 1.62% lower than that obtained by the spring constant of 3 N/m. After considering the contact deformation, the average Young's modulus for Au NWs increases by 4.63%, 4.45% and 4.71% with the cantilever's spring constant being 3 N/m, 3.017 N/m and 2.983 N/m, respectively. We can see that the value of cantilever's spring constant exerts a negligible effect on the Young's modulus value and the value added due to the consideration of contact deformation.

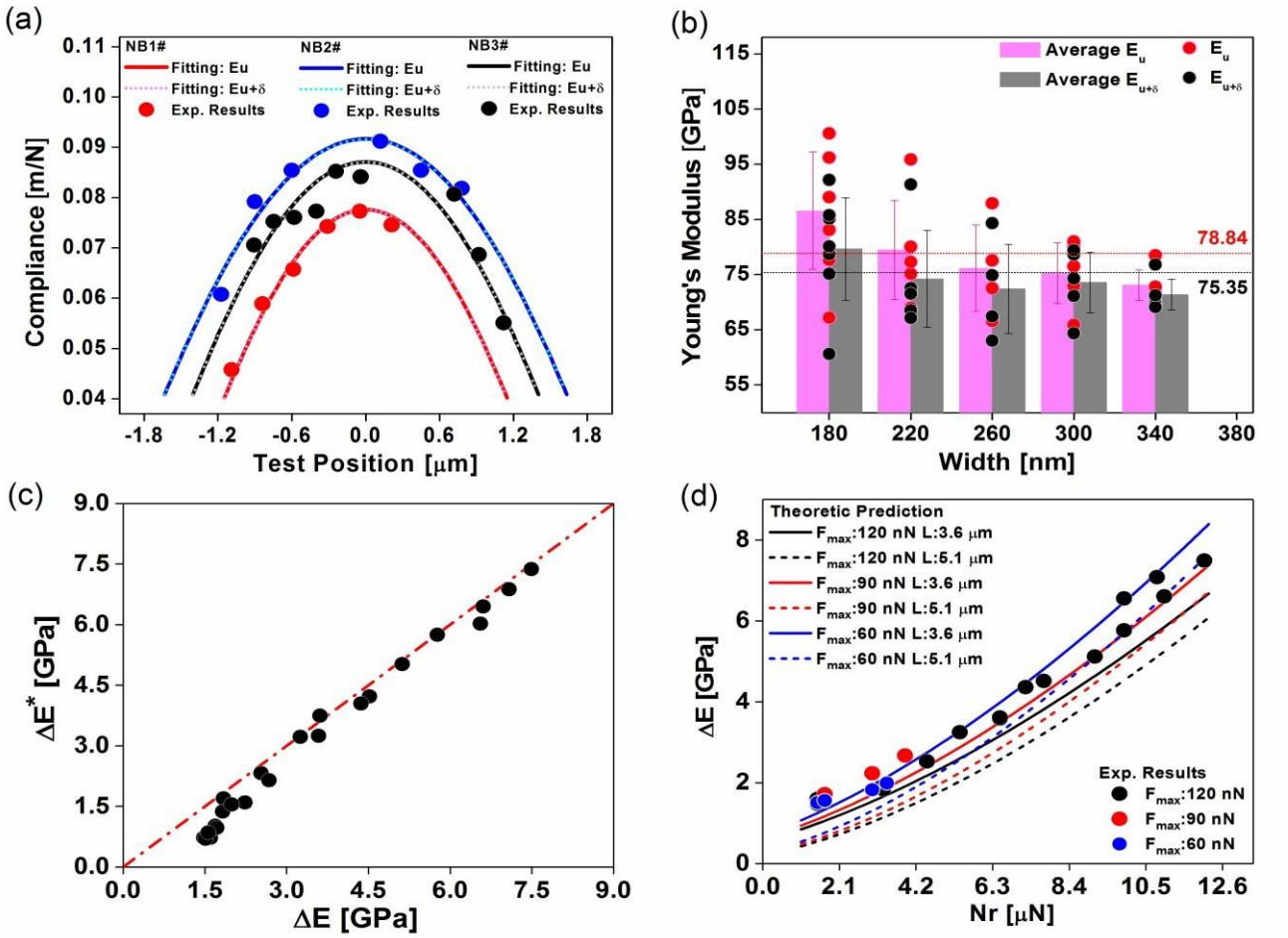

Figure 3 (a) Experimental data and fitting curves of compliance–test position relationships based on the TN–NB test combined model considering (solid line) and neglecting (short dotted line) the effect of contact deformation for three different Au NB samples (NB 1#: length (L): 4.1 μm, width (w): 260 nm, F_{max}: 120 nN, N_r:9.1 μN, E_u: 72.53 GPa, $E_{u+\delta}$: 67.43 GPa. NB 2#: L: 5.1 μm, w: 220 nm, F_{max}: 120 nN, N_r: 11 μN,

E_u: 75.15 GPa, $E_{u+\delta}$: 68.5 GPa. NB 3#: L: 4.6 μm, w: 220 nm, F_{max}: 120 nN, N_r: 9.9 μN, E_u:77.33 GPa, $E_{u+\delta}$: 71.38 GPa.). (b) Plots of the experimentally evaluated Young's moduli versus the NB width. The red and black solid circles denote the results considering and ignoring the influence of contact deformation, respectively; the averages are plotted as dashed lines. The column bars are plots of the averaged Young's modulus against the NB width considering (pink) and ignoring (grey) the influence of contact deformation. (c) Plots of the theoretical calculated Young's modulus variation ΔE^* versus the experimental evaluated Young's modulus variation ΔE for each tested sample. (d) The solid circles are plots of the experimentally evaluated Young's modulus variation ΔE against the residual force N_r for each tested Au NB sample. The curves are theoretical predicted relationships between ΔE and N_r under given experiment conditions based on the TN–NB test combined model.

To provide guidance on decreasing the effect of contact deformation on the NB test, the effects of N_r, L, F_{max}, Γ and E_u on ΔE are calculated separately following the TN–NB test combined model. In Figure 3(d), the theoretical predicted $N_r - \Delta E$ relationship for different experiment conditions are plotted as curves and the experimentally evaluated values are plotted as solid circles. Both theoretical predictions and experimental results suggest that the influence of contact deformation is more severe for larger residual forces. To avoid the influence of contact deformation, it is advisable to subject the bending test to sufficient aging, considering that the residual force is released as the aging time increases. The influence of the sample length L, the maximum applied load F_{max} and the work of adhesion Γ on ΔE is demonstrated in Figure S6 in the ESI. The results suggest that for NWs with the same material, the effect of contact deformation is greater for samples with smaller lengths, and that the external applied load should be as large as possible to reduce the influence of contact deformation.

As the work of adhesion Γ increases, ΔE also shows a tendency to decrease. However, the effect of changing Γ and L on the variation of ΔE in the test range of these parameters is negligible compared with the changing N_r and F_{max}. The effects of Γ, L, N_r and F_{max} on ΔE are monotonic, while the effect of the actual Young's modulus E_u on ΔE is quite complicated. For some test systems, the influence of E_u on ΔE may account for the experimentally obtained variances in the size dependency of Young's modulus. As shown in Figure S7 in the ESI, as E_u increases, ΔE first decreases then increases, and the value of E_u corresponding to the minimum of ΔE remains constant with the increase of F_{max} and shifts positively with the increase of L and N_r. The non-monotonic effect of E_u on ΔE can be easily understood in the case of the single center bending NB test, where ΔE can be expressed as $\Delta\rho \times \partial E/\partial\rho$[20]. As shown in Figure S8 in the ESI, as E_u increases, $\partial E/\partial\rho$ and $\Delta\rho$ increases and decreases, respectively. These theoretical analyses provide clear guidance for selecting experiment conditions that avoid the influence of contact deformation on the assessment of Young's moduli and understanding the variances in the experimentally obtained size dependency of Young's moduli for 1D nanomaterials.

In NB tests on various NW samples, the parameters of variation include the width (w), suspended length (L), residual force (N_r) and true Young's modulus (E_u) of the NWs. The specific values of w, L, N_r, F_{max}, E_u, $E_{u+\delta}$ and ΔE ($\Delta E = E_u - E_{u+\delta}$) of each tested Au NB sample are summarized in Table 1.

To demonstrate further the reliability and accuracy of the developed methodology, we introduce the theoretically calculated Young's modulus variation, ΔE^*, and plot ΔE^* versus ΔE in Figure 3(c). The theoretical variation is basically consistent with the measured variation and the maximum

variation is about 7.5 GPa, about ten percent of the averaged Young's modulus. Linear fitting the data with $\Delta E = \Delta E^*$ gives the standard deviation of 0.50 GPa, thereby illustrating the reliable methodology for mechanical characterization of nanomaterials.

Conclusions

The present work experimentally and theoretically investigated the influence of adhesion contact deformation on the NB test. The theoretical analysis is based on the adhesion contact deformation TN model and considering the deformation of the supporting base at the two clamped ends of a tested NB. Taking the adhesion contact deformation into account increases the average Young's modulus, for the tested Au NWs with widths ranging from 180 to 340 nm, from 75.35±7.87 GPa to 78.84±9.42 GPa, which is consistent with the reported value of Au bulk Young's modulus25. The present work provides the guideline how to make the NB tests more reliable, especially how to analyze the effect of adhesion contact deformation in the NB tests. The reported Young's moduli of Si[27], CuO[46], ZnO[12], Ag[47], etc nanomaterials are size-dependent. The highly reliable and accurate method developed in this paper is able to explore the size-dependent Young's modulus at the nanoscale for all nanomaterials. In addition, the finding of adhesion contact induced plastic deformation deserves systematically study, especially atomistic simulations. The developed methodology of NB tests will be combined with electrochemistry in order to investigate the interactions among surface stress, charge, and adhesion.

Table 1. Experimental evaluated and theoretical predicted Young's modulus variation for each tested Au NB sample.

F_{max}(nN)	L(μm)	w(nm)	N_r(μN)	$E_{u+\delta}$(GPa)	E_u(GPa)	ΔE(GPa)
120	4.1	260	6.5	63.025	66.61	3.59
120	4.1	260	9.1	67.425	72.55	5.12
120	3.6	260	6.5	84.3	87.91	3.61
120	5.1	220	11.0	68.525	75.13	6.61
120	5.1	220	12.1	72.54	80.03	7.49
120	4.6	220	7.7	91.35	95.87	4.52
120	4.6	220	9.9	71.55	77.32	5.77
120	3.6	220	3.3	67.15	68.99	1.84
120	5.1	180	9.9	60.625	67.18	6.56
120	5.1	180	10.8	85.125	92.21	7.08
120	4.6	180	7.2	78.725	83.09	4.36
120	4.1	180	4.5	75.125	77.66	2.53
120	4.1	180	7.2	80.135	96.19	16.06
120	3.6	180	5.4	85.77	89.02	3.25
120	3.6	180	4.5	92.14	100.57	8.43
120	4.6	340	1.7	70.125	71.68	1.55
120	4.6	300	1.5	78.625	80.11	1.48
120	4.6	300	1.5	79.4	81	1.60
60	4.6	260	3.9	74.875	77.55	2.68
60	4.6	300	3.0	74.3	76.54	2.24
60	4.6	340	1.7	76.8	78.49	1.69
60	4.6	340	1.7	69.6	71.32	1.72
90	4.6	300	3.0	71.125	72.95	1.83
90	4.6	300	1.5	64.375	65.89	1.51

90	4.6	340	3.4	69.125	71.12	1.99
90	4.6	340	1.7	71.25	72.81	1.56

Acknowledgements

This project was funded by research grants (No. 15DZ2260300 and No. 16DZ2260600) from the Science and Technology Commission of Shanghai Municipality, China, and research grant from the Hong Kong Polytechnic University (1-99QP), Hong Kong, China. The authors appreciated the technical assistance from the Materials Characterization and Preparation Facilities and the Nanoelectronic Fabrication Facility at HKUST.

Notes and references

1. X. Dai, A. Messanvi, H. Zhang, C. Durand, J. Eymery, C. Bougerol, F. H. Julien and M. Tchernycheva, *Nano letters*, 2015, **15**, 6958-6964.

2. X. Lu, G. Wang, T. Zhai, M. Yu, S. Xie, Y. Ling, C. Liang, Y. Tong and Y. Li, *Nano letters*, 2012, **12**, 5376-5381.

3. G. Zhu, R. Yang, S. Wang and Z. L. Wang, *Nano letters*, 2010, **10**, 3151-3155.

4. Z. Wang and J. Song, *Science*, 2006, **312**, 242 - 246.

5. T. Sekitani, in *Stretchable Bioelectronics for Medical Devices and Systems*, Springer, 2016, pp. 133-149.

6. C. M. Lieber and Z. L. Wang, *Mrs Bulletin*, 2007, **32**, 99-108.

7. K. Eom, H. S. Park, D. S. Yoon and T. Kwon, *Phys. Rep.-Rev. Sec. Phys. Lett.*, 2011, **503**, 115-163.

8. J. H. Bak, Y. D. Kim, S. S. Hong, B. Y. Lee, S. R. Lee, J. H. Jang, M. Kim, K. Char, S. Hong and Y. D. Park, *Nature materials*, 2008, **7**, 459-463.

9. M. J. Gordon, T. Baron, F. Dhalluin, P. Gentile and P. Ferret, *Nano letters*, 2009, **9**, 525-529.

10. C. Q. Chen, Y. Shi, Y. S. Zhang, J. Zhu and Y. J. Yan, *Physical Review Letters*, 2006, **96**, 075505.

11. A. Asthana, K. Momeni, A. Prasad, Y. K. Yap and R. S. Yassar, *Nanotechnology*, 2011, **22**, 265712.

12. R. Agrawal, B. Peng, E. E. Gdoutos and H. D. Espinosa, *Nano letters*, 2008, **8**, 3668-3674.

13. F. W. DelRio, C. Jaye, D. A. Fischer and R. F. Cook, *Applied Physics Letters*, 2009, **94**, 131909.

14. H. Xu and G. Pharr, *Scripta Materialia*, 2006, **55**, 315-318.

15. Y. Calahorra, O. Shtempluck, V. Kotchetkov and Y. E. Yaish, *Nano letters*, 2015, **15**, 2945-2950.

16. Y. J. Kim, K. Son, I. C. Choi, I. S. Choi, W. I. Park and J. I. Jang, *Advanced Functional Materials*, 2011, **21**, 279-286.

17. C.-C. Roehlig, M. Niebelschuetz, K. Brueckner, K. Tonisch, O. Ambacher and V. Cimalla, *Physica Status Solidi B-Basic Solid State Physics*, 2010, **247**, 2557-2570.

18. B. Wen, J. E. Sader and J. J. Boland, *Physical Review Letters*, 2008, **101**.

19. Y. Chen, B. L. Dorgan, D. N. McIlroy and D. Eric Aston, *Journal of Applied Physics*, 2006, **100**, -.

20. Y. Gao, Y.-J. Sun and T.-Y. Zhang, *Applied Physics Letters*, 2016, **108**, 123104.

21. W. K. Chan, J. Li, Y. Wang, S. Zhang and T. Zhang, *Acta Mech. Solida Sin.*, 2010, **23**, 283-296.

22. H.-Y. Huang, Z.-Y. Li, J.-Y. Lu, Z.-J. Wang, C.-S. Wang, K.-M. Lau, K. J. Chen and T.-Y. Zhang, *Journal of micromechanics and microengineering*, 2009, **19**, 095019.

23. Y. Ding, P. Zhang, Z. Long, Y. Jiang, J. Yin, F. Xu and Y. Zuo, *Journal of Alloys and Compounds*, 2009, **474**, 223-225.

24. B. Wu, A. Heidelberg and J. J. Boland, *Nature materials*, 2005, **4**, 525-529.

25. W. D. Callister's, 2010.

26. X. Li, H. Gao, C. J. Murphy and K. Caswell, *Nano letters*, 2003, **3**, 1495-1498.

27. X. X. Li, T. Ono, Y. L. Wang and M. Esashi, *Applied Physics Letters*, 2003, **83**, 3081-3083.

28. T. Y. Zhang and J. Hack, *physica status solidi (a)*, 1992, **131**, 437-443.

29. X. Zhou, H. Ren, B. Huang and T. Zhang, *Science China Technological Sciences*, 2014, **57**, 680-691.

30. T.-Y. Zhang, M. Luo and W. K. Chan, *Journal of applied physics*, 2008, **103**, 104308.

31. M. A. Mahmoud, D. O'Neil and M. A. El-Sayed, *Nano letters*, 2014, **14**, 743-748.

32. K. Smaali, S. Desbief, G. Foti, T. Frederiksen, D. Sanchez-Portal, A. Arnau, J. Nys, P. Leclère, D. Vuillaume and N. Clément, *Nanoscale*, 2015, **7**, 1809-1819.

33. T.-Y. Zhang, in *Micro and nano mechanical testing of materials and devices*, Springer, 2008, pp. 209-279.

34. K. Johnson, *Journal*, 1974.

35. K. L. Johnson, K. Kendall and A. D. Roberts, *Proceedings of the Royal Society of London A: Mathematical, Physical and Engineering Sciences*, 1971, **324**, 301-313.

36. B. V. Derjaguin, V. M. Muller and Y. P. Toporov, *Journal of Colloid and Interface Science*, 1975, **53**, 314-326.

37. C. Thornton and Z. Ning, *Powder Technology*, 1998, **99**, 154-162.

38. D. Maugis and H. Pollock, *Acta Metallurgica*, 1984, **32**, 1323-1334.

39. L. Kogut and I. Etsion, *Journal of Colloid and Interface Science*, 2003, **261**, 372-378.

40. J. Wachtman Jr, W. Tefft, D. Lam Jr and C. Apstein, *Physical review*, 1961, **122**, 1754.

41. T. Y. Zhang, Y. J. Su, C. F. Qian, M. H. Zhao and L. Q. Chen, *Acta Materialia*, 2000, **48**, 2843-2857.

42. S. Das, P. Sreeram and A. Raychaudhuri, *Nanotechnology*, 2007, **18**, 035501.

43. G. Ahmadi, *Fluid Mechanics of Aerosols. Clarkson University*, 2005, **24**.

44. K. E. Petersen, *Proceedings of the IEEE*, 1982, **70**, 420-457. 45. H. D. Espinosa and B. C. Prorok, *Journal of Materials*

Science, 2003, **38**, 4125-4128.

46. E. P. S. Tan, Y. Zhu, T. Yu, L. Dai, C. H. Sow, V. B. C. Tan and C. T. Lim, *Applied Physics Letters*, 2007, **90**, -.

47. G. Jing, H. Duan, X. Sun, Z. Zhang, J. Xu, Y. Li, J. Wang and D. Yu, *Physical Review B*, 2006, **73**, 235409.